Tear Strength of Styrene−Butadiene−Styrene Block Copolymers

Chi Wang†

Department of Chemical Engineering, National Cheng Kung University, Tainan 701-01, Taiwan

Received June 22, 2001

ABSTRACT: Measurements of tear strength were carried out on specimens of styrene−butadiene−styrene (SBS) block copolymers prepared from three formation conditions: SBS_I cast from toluene solution; SBS_{II} and SBS_{III} hot-pressed from molten state. Prior to hot press, SBS_{III} were additionally melt processed in an internal mixer. Results showed that stick−slip tearing was observed at all given rates of tearing. SBS_{II} and SBS_{III} possessed similar tear strengths, ca. 24.2 ± 2.6 kJ/m^2, which was about 2 times larger than that for SBS_I, ca. 14.3 ± 1.5 kJ/m^2. Moreover, SBS_{III} possessed the largest elastic modulus, ca. 6 times larger than that of SBS_I whose elastic modulus was the lowest. Microstructure and properties of PS and PB phases were extensively studied using transmission electron microscopy (TEM), small-angle X-ray scattering (SAXS), and thermal and dynamic mechanical analyses. SAXS and TEM results showed that the interdomain length and the diameter of PS cylinders were remained approximately similar, 28.6 ± 2.5 and 12.7 ± 2.5 nm, respectively, regardless of sample preparation. Relatively ordered microdomains of PS cylinders packed hexagonally were developed in SBS_I, whereas a more continuous pack of interconnected PS cylinders was observed in SBS_{II} and SBS_{III}. On tearing, the presence of interconnected PS cylinders is more likely to blunt the crack tip, leading to a rough fracture locus which accounts for a larger energy required to fracture hot-pressed specimens. Compared to SBS_{II}, the enhanced elastic modulus for SBS_{III} was attributed to a shortening of the PB molecular segments between effective cross-linkers (M_c) determined by equilibrium swelling of the network using isooctane. Changes of the molecular weight distribution of SBS_{III} due to the stress-induced degradation of SBS molecules were revealed by gel permeation chromatography. It implies that original SBS molecular chains would undergo intensive shear stresses (friction) in the mixer and mechanochemical degradation of triblock components takes place, giving rise to the reduction of M_c.

Introduction

Polymer chain sequences with different repeating units can be chemically linked together through covalent bonds to form a block copolymer. When two immiscible constituents are selected to form the block copolymers, phase separation takes place and results in the formation of microdomains with sizes of ca. several tens of nanometers. To obtain good mechanical properties in practical application, one of the constituents is normally in the glassy state (rigid segments) at the service temperatures and forms the dispersed microdomains. Soft segments, on the other hand, in the rubbery state are intervening between the rigid microdomains to be responsible for the elastic behavior. The rigid microdomains serve as fillers and play a role as physical cross-linkers as well. Thus, the novel block copolymers termed thermoplastic elastomers can be regarded as filler-reinforced rubbery composites with the ability to flow at temperatures higher than the glass transition of the rigid phase.

By controlling appropriately the segment length (or molecular weight) of each constituent in the polymeric chains, block copolymers possess very unique properties, especially the excellent elasticity at ambient temperature and flowability at elevated temperatures. There are many articles in the literature to discuss the microdomain formation and its morphology.[1−7] The microdomain morphology of block copolymers depends not only on the relative volume fraction of the constituents (thermodynamic effects) but also on the processing circumstances (dynamic effects). It is generally recognized that the apparent mechanical properties are closely related to the microdomain morphology developed in the specimens. From a composite point of view, not only the filler content but also the shape (morphology) of the fillers can significantly influence the composite performance.

Styrene−butadiene−styrene (SBS) block copolymers are a novel thermoplastic elastomer that offers interesting possibilities for studying the relation between phase behavior and microstructure development. In the past three decades, a considerable amount of research has been aimed at gaining a better understanding of microdomain morphology,[1−7] microdomain size,[5,8,9] interface of the microdoamin,[10−13] order−disorder transition,[14,15] order−order transition,[16−18] and the deformation and orientation of microdomains.[19−22] On the other hand, tear strength and the associated fracture mechanism have received less attention.

In our recent article,[23] the tear strengths of SBS specimens cast from toluene, cyclohexane, and THF/MEK solutions have been investigated. Results showed that the level of toughness is mainly dependent on the microdomain morphology which is closely associated with the polymer−solvent interactions, leading to the difference in the degree of swelling of polymer segments and hence the effective volume fraction of each phase. SBS specimens cast from THF/MEK possess a microstructure of more continuous PS microdomains which accounts for the yielding behavior under tensile tests and enhanced strength on tearing.

The objective of the present study is to gain a better understanding of the factors that are essential for the toughness determination of the SBS block copolymers. The detailed microstructure developed under different formation conditions is investigated using various techniques. Finally, the tear strength is correlated with the microstructure to reveal the fracture behavior.

† Fax +886-6-2344496; E-mail chiwang@mail.ncku.edu.tw.

10.1021/ma011077q CCC: $20.00
Published on Web 11/20/2001

Experimental Section

Materials and Sample Preparation. The SBS block copolymer used was obtained from Shell Co. Ltd., and the weight ratio of styrene/butadiene is 28/72 according to the NMR measurements. To characterize the molecular weight, the as-received SBS block copolymers were dissolved in THF and analyzed by gel permeation chromatography (GPC) using a calibration curve determined tentatively from PS standards. The weight-average molecular weight (M_w) of the as-received copolymers is 1.36×10^5 g/mol. The weight ratio of triblock to diblock determined from the GPC curve (as shown by the SBS_I curve in Figure 8) is about 78/22, and the weight-average molecular weight for the triblock and diblock are ca. 1.38×10^5 and 7.3×10^4 g/mol, respectively. Therefore, the sequence weights for the triblock and diblock are estimated to be 19300S−99400B−19300S and 20400S−52600B, respectively. The molecular weight of PS sequence is similar in diblock and triblock, but the molecular weight of PB sequence in triblock is about 2 times that in diblock.

Specimens were prepared from three different conditions and denoted as SBS_I, SBS_{II}, and SBS_{III}, respectively. SBS_I specimens about 0.8 mm thick were prepared by solution casting from 20 wt % toluene solution on a Teflon mold. After the solvent was slowly evaporated at room temperature for several days, the cast specimens were subsequently dried at 60 °C under vacuum until a constant weight was reached. To prepare SBS_{II} specimens, hot press of the SBS pellets was carried out at 120 °C and 0.6 MPa to melt the copolymers for 20 min, followed by a slow cooling to room temperature under atmosphere. The same conditions for hot press were also applied to prepare SBS_{III} specimens. Prior to the hot press, however, the raw SBS block copolymers were melt processed in a Brabender internal mixer additionally. Internal mixers have been widely used for plastics compounding and elastomer kneading due to the good mixing performance. Effects of the additional melt process in the mixer can be revealed by any difference in mechanical performance between SBS_{II} and SBS_{III} specimens. The investigation on SBS_{III} specimens (effect of melt mixing) forms a preliminary study for SBS/PS blend systems, which is currently carried out in this laboratory. The rotor speed and the temperature in the mixer chamber were tentatively set to be 25 rpm and 110 °C to avoid the thermal degradation of the PB phase. Antioxidant (Irganox 1010, Ciba-Geigy Co.) of 1 phr content was added to SBS melt of 40 g during mixing process, and the period of mixing was 30 min.

To monitor any change in SBS chain characteristics due to processing, the molecular weight distribution of the as-prepared specimens (SBS_I, SBS_{II}, and SBS_{III}) was measured via GPC again.

Measurements of Tear Strength and Tensile Properties. The Trouser tear test was carried out to determine the tear strength of SBS block copolymers. Backing cloth was embedded in the strip specimens (100 mm long, 20 mm wide) to minimize the extension and creep phenomena of specimens.[24] The spacing between two cloth was about 2.5 mm. To prevent a tear deviation, the strip specimen was scored on one side with a razor blade along the centerline to a certain depth. Thus, about 0.5 mm thickness was remained to be torn through. The tear strength (G_c) is calculated through eq 1,[24]

$$G_c = 2f/t \tag{1}$$

where f is the force to propagate a tear and t is the torn thickness measured using a reflection microscope after the tear test. The tear strength can be considered as the fracture energy per unit area required to propagate the growing crack. Measurements of the tear strength were carried out at room temperature using different rates of tear (R) from 3.3 to 8.3×10^3 μm/s. Each experimental result was an average of five tear tests.

The tensile properties of specimens were determined using Instron tensile testing machine equipped with an extensometer. Dumbbell-shaped specimens with a gauge length and a width of 10 and 4 mm were stretched with a strain rate of 8.3×10^{-3} s^{-1} at room temperature. Strain energy density at break, U_b', was determined from the area under the stress−strain curve. The elastic modulus, E, was measured from the linear slope at small strains. Breaking stress (σ_b) and breaking strain (ϵ_b) were measured as well.

Microdomain Observations. The morphology of microdomains developed in the specimens was examined by transmission electron microscopy (TEM) and small-angle X-ray scattering (SAXS). For TEM observation, ultrathin sections of ∼50 nm were prepared using an ultramicrotome (LEICA ULTRACUT UCT) operated at cryo conditions. To obtain the three-dimensional structure, the ultrathin sections normal and parallel to the sample surface were prepared to reveal the details of the microdomain (edge-view image and through-view image, respectively). The ultrathin sections were immersed in 1% (w/v) solution of osmium tetroxide (OsO_4) for 20 min to stain the PB phase of SBS. Electron microscopy observation was carried out with a JEOL JEM-2010 transmission electron microscope operated at 200 kV. SAXS experiments were conducted with Cu radiation from an apparatus[25] consisting of a 18 kW Rigaku rotating anode X-ray generator operated at 40 kV and 200 mA. Monochromation of the incident X-ray beam was carried out by a pyrolytic graphite. Three pinhole collimators with a diameter of 1 mm were used, and the sample-to-detector distance was 2270 mm. The incident X-ray beam was normal the sample surface, and the intensity profiles of the through-view pattern were obtained using a two-dimensional position-sensitive detector with 256×256 channels to cover an active area of 20×20 cm^2. The exposure time was 1 h for each measurement.

Phase Transition Measurements. To determine the glass transitions of the constituents, calorimetric measurements were performed on a differential scanning calorimeter (DSC, Du Pont 910). A constant heating rate of 10 °C/min was employed to heat the SBS specimens from −130 to 130 °C. To reveal the transition of PS phase and the disruption of the microdomains, rheological experiments were also conducted using a dynamic mechanical spectrometer (RDAII, Rheometrics Inc.) operated with a parallel-plates modulus. Temperature sweep from 50 to 150 °C was carried out using a rate of 3 °C/min at a given frequency of 1 Hz. The dynamic storage (G') and loss (G'') moduli and the deduced loss tangent ($\tan \delta = G''/G'$) were determined for specimens subjected to a 1% shear strain amplitude. The transition of the PB phase was further investigated using a DMA7e apparatus (Perkin-Elmer Co.) operated on a three-point-bending mode to measure the dynamic storage (E') and loss (E'') moduli. Upon heating from −130 to 50 °C at a rate of 3 °C/min, the specimens were oscillated at a fixed frequency of 1 Hz. The corresponding tan δ ($=E''/E'$)was determined for specimens as a function of temperature.

Measurements of Molecular Weights between Cross-links. The molecular weights of PB segments between physically cross-linked microdomains (and entanglements) were measured using an equilibrium swelling method. Being a good solvent for PB but nonsolvent for PS, isooctane was used to immerse the SBS specimens to swell the PB phase. The weight increase of specimens due to the absorption of isooctane was monitored continuously. Since the weight fraction of the PB phase in SBS was 0.72, the volume fraction of PB (ϕ_2) in the swollen network was determined by

$$\phi_2 = \frac{0.72 W_{SBS}/\rho_{SBS}}{0.72 W_{SBS}/\rho_{SBS} + W_s/\rho_s} \tag{2}$$

where W_{SBS} was the dry SBS weight, W_s was the uptake weight of isooctane at equilibrium swelling, and ρ_{SBS} and ρ_S were the densities of SBS and isooctane, respectively. Cross-link density (ν) was determined as follows:[26]

$$\nu = \frac{-\rho_s[\ln(1-\phi_2) + \phi_2 + \chi\phi_2^2]}{\phi_2^{1/3} - \phi_2/2} \tag{3}$$

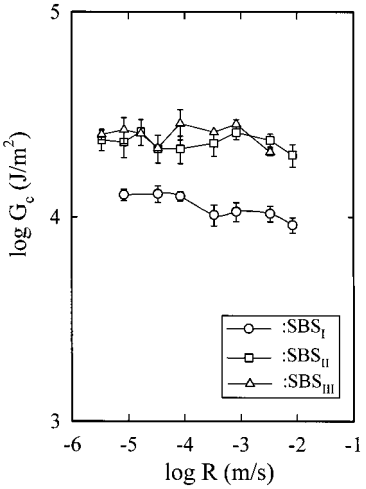

Figure 1. Variation of tear strength, G_c, with tearing rate, R, for specimens prepared from different conditions.

where χ was the interaction parameter of PB/isooctane pairs,[27] taken to be $0.406 + 0.522\ \phi_2$. Thus, the average molecular weight of PB segments between PS microdomains, M_c, was estimated to be ρ_2/ν, where ρ_2 is the density of PB.

Results and Discussion

Tear Strength and Tensile Properties. In this study, the stick−slip phenomenon was always observed on tearing all SBS specimens. Stick−slip tearing is attributed to the heterogeneity within the specimens due to the presence of microdomains which deviates the crack growing tip,[23] leading to an anisotropic nature at the crack tip. When stick−slip tearing took place, the minimum tearing force[28] was essentially taken to calculate the strength using eq 1, and the speed of the cross-head movement was used to represent the apparent tearing rate. Figure 1 shows the effect of apparent tearing rate R on the tear strength of SBS prepared from different formation conditions. It seems that tear strength is independent of the apparent tearing rate. It is in contrast with results[29] obtained from steady tearing of general elastomers, of which the tear strength increases with increasing rates of tearing. It is evident that both SBS_{II} and SBS_{III} possess a similar tear strength, ca. 24.2 ± 2.6 kJ/m^2. On the other hand, a lower tear strength ca. 14.3 ± 1.5 kJ/m^2 is obtained for SBS_I. Depending on the preparation methods, it is intriguing to note that about 2 times difference in the measured tear strength can be obtained.

The typical stress−strain curves measured at a strain rate of 8.3×10^{-3} s^{-1} are shown in Figure 2. The deduced elastic modulus, breaking stress, breaking strain, and apparent strain energy density at break for different SBS specimens are tabulated in Table 1. Each value was obtained from the average of five individual tensile tests. Although the breaking strain is similar in all three specimens, the breaking stress of SBS_I is 2.2 times larger than that of SBS_{II} and even 4.5 times larger than SBS_{III}. This may be related to the reduction of entanglements in the PB phase and well-developed PS microdomains in SBS_I specimens due to a near equilibrium process of phase separation for both constituents (as discussed below). For specimens with well-developed microdomains, the fragmentation and reorientation of the PS microdomains take place at low to moderate strains, followed by the molecular orientation of PB segments at high strains.[19] Indeed, a pronounced upturn

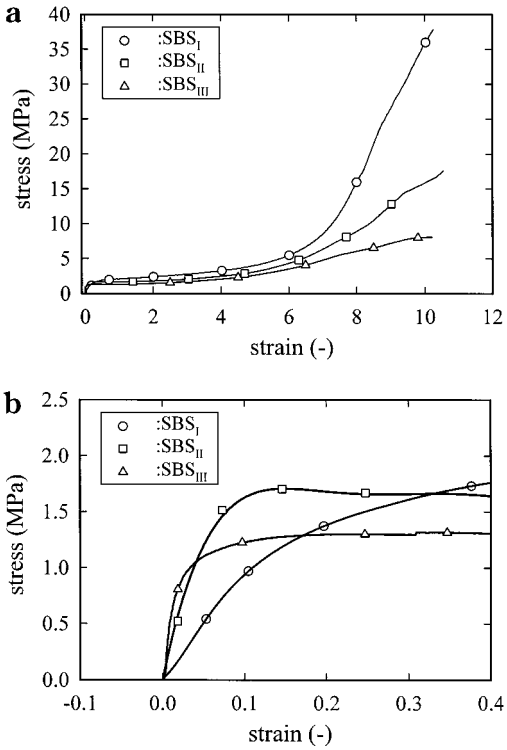

Figure 2. (a) Typical stress−strain relation for specimens prepared from different conditions and (b) enlarged portion of (a) at small strains.

Table 1. Stress−Stain Results and Crack Tip Diameter, *d*, Measured at Room Temperature and a Strain Rate of 8.3 × 10^{-3} s^{-1}

code	E (MPa)	σ_b (MPa)	ϵ_b	U_b' (MJ/m^3)	d (mm)
SBS_I	11.7 ± 0.6	37.9 ± 1.0	10.3 ± 0.5	98 ± 9	0.15
SBS_{II}	41.6 ± 1.5	17.2 ± 0.2	10.6 ± 0.5	63 ± 2	0.38
SBS_{III}	69.1 ± 1.4	8.4 ± 0.4	10.0 ± 0.4	36 ± 2	0.67

of stress at a large strain, ca. 7.0, is detected for SBS_I, as shown in Figure 2. The upturn of stress implies the presence of small fragmented PS microdomains, bridging by PB chains that have been extremely stretched. It has been pointed out that a more continuous PS dispersed phase will result in the reduction of the breaking stress.[23] In the extreme case, yielding takes place when the lamellar microstructure is developed. The yielding phenomenon is not observed here in all three kinds of specimens which implies the absence of lamella-like microstructure. Another interesting feature is the 4−6 times difference in the elastic moduluous resulting from different sample preparation. Hot-pressed specimens have a larger elastic modulus than that of specimens cast from toluene solution. Moreover, the additional melt process in an internal mixer results in an increase of elastic modulus to 69.1 MPa, compared to the one without that process, 41.6 MPa.

For each specimen, the strain energy density at break U_b' was determined from the area under the stress−strain curve in Figure 2. A relatively larger U_b' is obtained for SBS_I, suggesting that a higher tear strength is required to fracture this specimen. Thomas[30] showed that the tear strength is quantitatively related to the strain energy density of the materials in the vicinity of the crack tip U_b as follows:

$$G_c = dU_b \tag{4}$$

where d is the diameter of the crack tip (or the size of

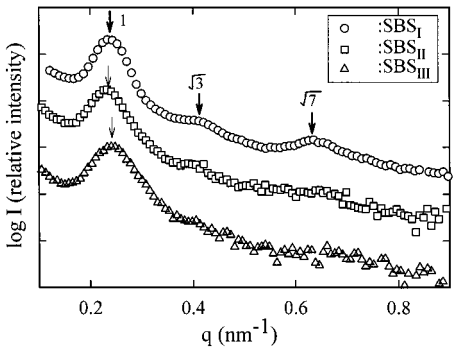

Figure 3. Small-angle X-ray scattering intensities, I, as a function of the scattering vector, q, for specimens prepared from different conditions (through-view scattering).

deformation zone at the crack tip). Gent et al.[31] have pointed out that the measured U_b' is much smaller, only about 10^{-4} times, than U_b for vulcanized elastomers due to the presence of accidental edge flaws in specimens for tensile tests. Nevertheless, the measured tear strength, according to eq 4, depends not only on the strain energy density but also on the diameter of the crack tip. The former is an intrinsic property of materials whereas the latter is associated with the fracture mechanism and the failure path. Therefore, tear strength can be enhanced when the failure locus is carefully controlled to render a blunt crack tip. "Knotty" tearing is such a fracture process to improve the toughness of elastomers after the carbon black is applied. Because of the difficulties in obtaining the U_b value, the measured U_b' was employed tentatively here to estimate the size of the deformation zone using eq 4. As shown in Table 1, it is interesting to note that the d value for SBS_I is about $^1/_3-^1/_5$ of that for SBS_{II} and SBS_{III}, although its intrinsic strength (U_b') is the largest. Thus, it is the deformation zone at the crack tip, rather than the intrinsic strength, dominates the level of tear strength of the as-prepared SBS specimens. Above observations lead us to conclude that the morphology of PS microdomains developed in the SBS specimens must play an important role in determining the tear strength and tensile properties as well. Detailed results for the microstructure of both PS and PB phases are given in the following sections. In the last section, correlations between the morphology and properties are provided.

Morphology of Microdomains. The volume fraction of PS phase was computed to be 0.24 from the weight fraction of the specimens by assuming a density for each microphase identical with that of the corresponding homopolymer, that is, 1.070 g/cm^3 for homo-PS and 0.882 g/cm^3 for homo-PB.[32] According to the volume fraction of the PS constituent, the equilibrium microdomain morphology is that of PS cylinders packed hexagonally.[33] Nevertheless, the actual structure of PS microdomains is dependent on the formation conditions as well from a dynamic point of view.

Figure 3 shows the SAXS profiles plotted against the scattering vector, q, which is given by $q = 4\pi/\lambda \sin(\theta/2)$, where λ and θ are the wavelength of X-ray and the scattering angle, respectively. The incident X-ray beam was normal to the sample surface (through-view scattering). Circular patterns of scattered X-ray intensities were obtained from the two-dimensional detector, implying that no preferential orientation of microdomains was developed globally. The profiles in Figure 3 are the averages of scattered intensities obtained at different azimuthal angles. Similar results were obtained but not shown here for brevity when the incident of X-ray beam was parallel to the sample surface (edge-view scattering). For SBS_I specimens, it may be seen that the ratio of intensity peak positions is $1:\sqrt{3}:\sqrt{7}$ for the three successive peaks. The Bragg peak at a relative position of $\sqrt{7}$ is typical for hexagonal arrangements of cylinders.[32,33] Thus, cylindrical PS microdomains in SBS_I specimens are likely to be packed hexagonally, which is confirmed by the corresponding TEM micrographs (Figure 4). The absence of the peak position at $\sqrt{4}$ predicted by theories and less prominent peaks at higher orders ($\sqrt{3}$ and $\sqrt{7}$) may indicate that perfect-equilibrium conditions for microstructure formation is difficult to achieve for this thick specimen (thickness of ca. 0.8 mm) although evaporation of toluene is carefully controlled to be sufficiently slow. For a well-ordered system with multiple diffraction peaks, the interdomain distance is given by $(4/3)^{1/2}(2\pi/q_{max})$ with the knowledge of the first scattering peak position, q_{max}. Thus, distance between adjacent PS cylinders is estimated to be 31.1 nm for SBS_I for a q_{max} value of 0.2336 nm^{-1}.

As shown in Figure 3, another feature of the SAXS patterns is the extinction of the higher order reflections for SBS_{II} and SBS_{III} specimens. The absence of multiple Bragg peaks may be interpreted in terms of deterioration of the long-range order when specimens are hot-pressed. In fact, irregular packing or interconnected microdomains of PS cylinders were observed from TEM micrographs (Figure 4). The scattering patterns of SBS_{II} and SBS_{III} specimens exhibit primary interaction peaks at scattering vectors of 0.2329 and 0.2404 nm^{-1}, respectively (Figure 3). Although there is no evidence of long-range ordering in the form of multiple Bragg peaks, the observed scattering maxima can be interpreted as a result of average interdomain distances($=2\pi/q_{max}$), resulting from short-range order interactions. Since the first peak position is more or less constant for all specimens (Figure 3), it is reasonable to assume that the distance between two adjacent PS cylinders is independent of the formation conditions and lies within the ranges of 26.1−31.1 nm.

Figure 4 gives the TEM micrographs for the SBS specimens obtained on the ultrathin sections cut parallel to the sample surface (through-view images). The dark regions correspond to the PB phases selectively stained with OsO_4 and the bright regions are associated with unstained PS microdomains. For SBS_I specimens, the image shows a grainy structure, within which PS cylinders are oriented parallel to each other. In some regions, orientation of PS cylinders normal to the sample surface is observed. The main microstructure of SBS_I consists of PS cylinders on a hexagonal-like array. It is consistent with the corresponding SAXS profile which shows the presence of $\sqrt{7}$ Bragg's peak (Figure 3). Globally, no preferential orientation of PS cylinders is found in the thick SBS_I specimens which leads to an isotropic character in mechanical strength under load. This is in contrast with microstructure obtained for thin specimens in which the perfect-equilibrium conditions for phase separation can be reached, and the PS cylinders are parallel to the sample surface.[32,33]

For hot-pressed specimens (SBS_{II} and SBS_{III}), on the other hand, the arrangement of microdomains is more distorted, and almost no presence of hexagonal arrays

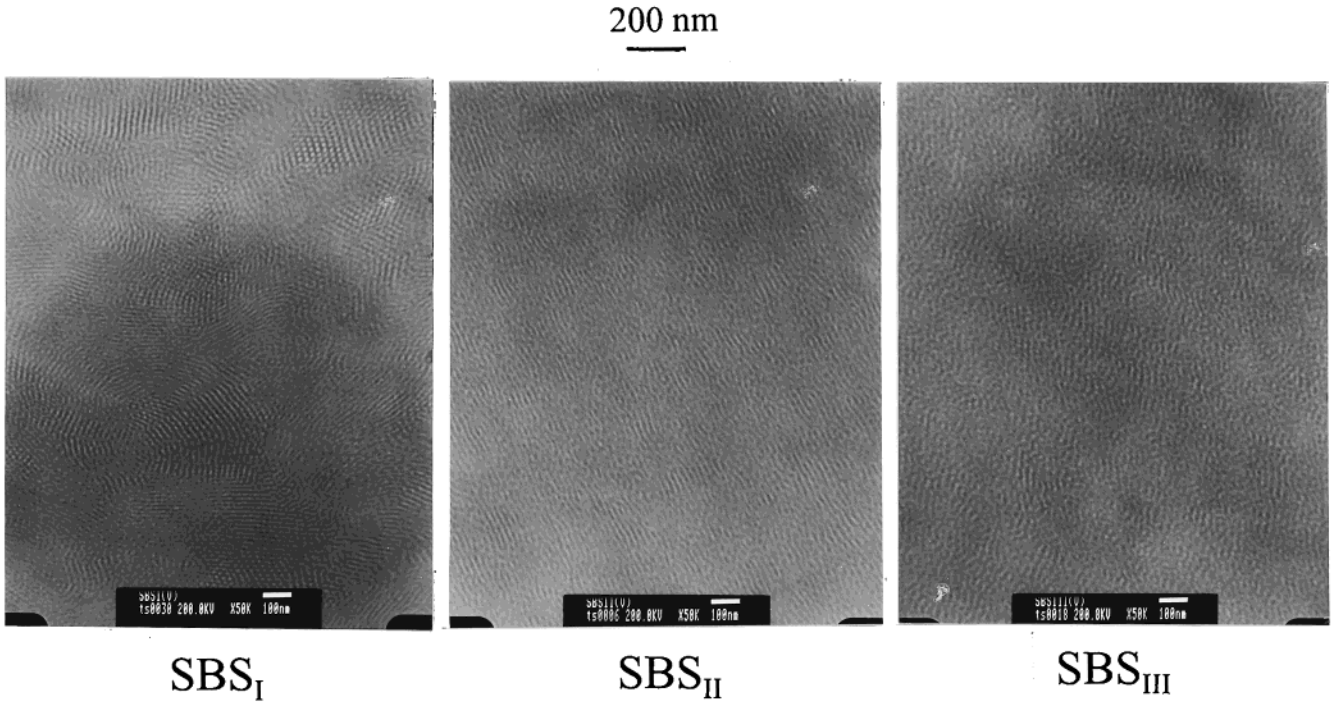

Figure 4. Transmission electron micrographs for specimens prepared from different conditions (through-view images, ×50K).

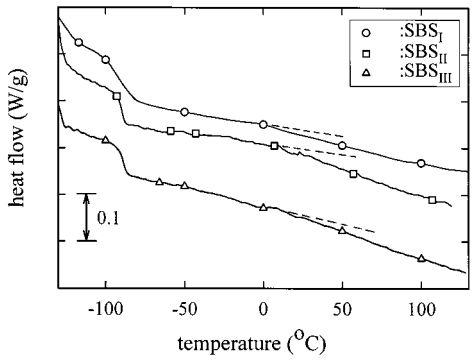

Figure 5. DSC heating scan (10 °C/min) for specimens prepared from different conditions.

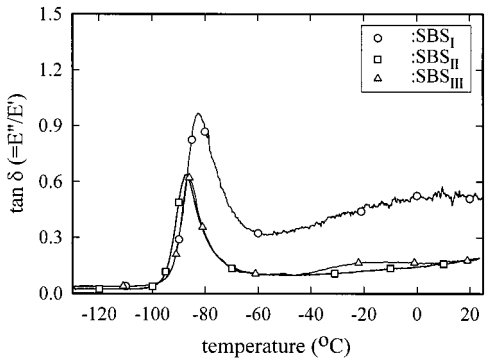

Figure 6. Plots of tan δ vs temperature to reveal the transition of PB phase in SBS specimens prepared from different conditions (DMA results).

of PS cylinders is observed in Figure 4 from the through-view image (also edge-view image, not shown here for brevity). It seems that both SBS_{II} and SBS_{III} have similar microdomain morphology with regions of either isolated or interconnected PS cylinders due to nonequilibrium conditions for phase separation to take place and proceed. This leads the disappearance of the higher-order Bragg peaks, compared to that of SBS_I, at $\sqrt{3}$ and $\sqrt{7}$ as shown in Figure 3. From the TEM images, it is evident that hot-pressed specimens show morphology with more continuous or interconnected PS cylinders than solution-cast specimens of which PS cylinders are packed in hexagonal-like arrangements. It should be noted that no grain consisting of PS cylinders uniaxially packed has been observed in SBS_{II} and SBS_{III}. Nevertheless, the diameters of the PS cylinders measured from TEM micrographs are approximately constant, being 12.6 ± 2.5, 12.7 ± 2.0, and 12.9 ± 1.8 nm for SBS_I, SBS_{II}, and SBS_{III} specimens, respectively.

Phase Transition. Figure 5 shows the DSC curves measured on SBS specimens at a heating rate of 10 °C/min. In all specimens, an evident glass transition of the PB phase is found but that for PS phase is not obvious. T_g values of the PB phase reported at the half-height of the corresponding heat capacity jump are independent of sample preparation: −88.9, −89.1, and −88.7 °C for SBS_I, SBS_{II}, and SBS_{III}, respectively. On the other hand, it seems that a broad glass transition for PS phase (indicated by the dashed lines in Figure 5) takes place from above 0 °C to the expected T_g value for homo-PS,[10,11] 98 °C calculated using the Fox equation and the corresponding PS molecular weight of ca. 2×10^4 g/mol. The T_g onset is about 0 °C for all three specimens. It has been widely discussed in the literature for the lowering and broad transition of T_g of the PS phase, compared to the neat homopolymers. Two general conclusions have been proposed to account for this anomalous transition: one is due to the asymmetric mixing,[10,11] and the other is attributed to the dynamic interactions[12,13] between PS and PB phases at the interface.

As shown in Figure 6 obtained from the DMA technique, the T_g determined from the positions of tan δ peaks are −84.7, −87.6, and −86.7 °C respectively for SBS_I, SBS_{II}, and SBS_{III} specimens. They are relatively higher than those measured by the DSC technique. Thus, different measurement techniques may give

Table 2. Results of Dynamic Mechanical Analyses Measured at 1 Hz and a Heating Rate of 3 °C/min

code	T_g of PB phase (°C)	value of tan δ peak for PB phase	E'(25 °C) (MPa)	E'(−125 °C)/E'(25 °C)
SBS_I	−84.7 ± 3.4	0.98 ± 0.04	17.3 ± 2.8	258
SBS_{II}	−87.6 ± 3.0	0.68 ± 0.04	39.0 ± 13.9	59
SBS_{III}	−86.7 ± 1.9	0.52 ± 0.12	52.8 ± 7.2	57

somewhat different T_g values, but a similar trend is obtained for T_g of the PB phase. On the basis of the DSC and DMA results, we conclude that no pronounced T_g shift for the rubbery phase in SBS specimens prepared from different approaches, except that a slightly high T_g is obtained for SBS_I measured by DMA. In addition to the T_g values, Table 2 also lists the other results measured from DMA, including tan δ peak values of the PB phase, dynamic storage modulus at 25 °C, E'(25 °C), and the ratio of dynamic storage modulus at −125 and 25 °C, E'(−125 °C)/E'(25 °C). It is of interest to note that a relatively larger tan δ value is obtained for SBS_I at the glass transition of PB phase compared to those for SBS_{II} and SBS_{III}, which have similar tan δ values. It implies that more rubberlike characteristics and pronounced viscoelastic effect due to the PB phase is expected in the SBS_I specimens compared to the others.

For the three SBS specimens, the relative magnitudes of E'(25 °C) are consistent with the elastic moduli obtained from the tensile test (Table 1). It should be noted that at 25 °C the PB phase is in the rubbery state, whereas the PS phase is in the glassy state. This suggests that the PS microdomains act like reinforced fillers dispersed in the PB rubbery matrix. Although different formation conditions were employed, the PS content and the diameter of PS cylinders were the same in all the three specimens, as discussed previously. From a composite point of view, the specimens with a more continuous PS morphology will give a larger E'-(25 °C) value due to a larger aspect ratio of the filler. At the temperature well below the glass transitions of both constituents, on the other hand, both PS and PB phases are in the glassy state, and the contribution to measured E'(−125 °C) is similar in all three specimens. It leads us to establish another guidance to estimate the continuity level of PS microdomains by using the ratio of E'(−125 °C)/E'(25 °C). The lower this ratio is, the more continuous morphology of the PS microdomains developed in the specimen. From Table 2, it is evident that SBS_I has the lowest E'(25 °C) and the largest E'(−125 °C)/E'(25 °C) ratio, suggesting that the connectivity of PS microdomains is the least in solution-cast specimens. This is in good agreement with the results obtained from TEM and SAXS.

To reveal the transition behavior of the PS phase from glassy state to terminal region, dynamic storage modulus (G') and dynamic loss modulus (G'') were measured from 50 to 150 °C at a fixed frequency of 1 Hz. Figure 7 gives temperature scans of loss tangent, tan δ(=G''/G'), for different specimens. A barely seen tan δ shoulder associated with the glass transition of PS phase is detected for SBS_{II} and SBS_{III} specimens at 86.8 ± 0.2 and 82.6 ± 2.7 °C, respectively. On the other hand, SBS_I exhibits a continuous increase of tan δ from 50 to 100 °C, giving no evident indication of PS T_g. Notice further that a broad and large tan δ peak is observed at temperatures above 110 °C for all three specimens. This large tan δ peak is relevant to the disruption of PS microdomain, and the corresponding temperature is

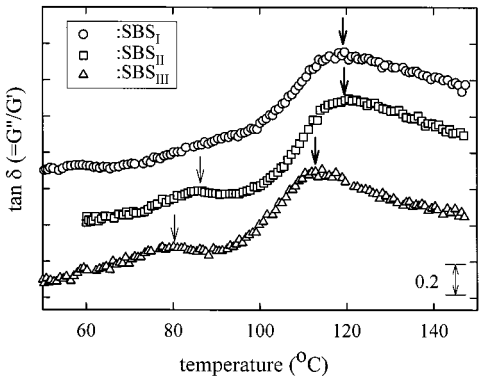

Figure 7. Plots of tan δ vs temperature to reveal the transition of PS phase in SBS specimens prepared from different conditions (RDAII results).

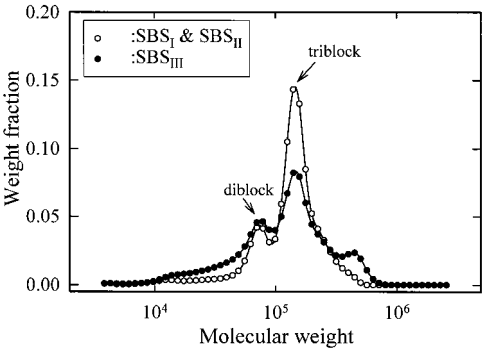

Figure 8. Molecular weight distributions of specimens prepared from different conditions (GPC results).

denoted to the domain disruption temperature,[34] T_{dd}. The domain disruption temperature is associated with the homogenization for the SBS copolymers where order−disorder transition[16−18,35] of microdomains takes place. In other words, complete dissolution of PS microdomains occurs when temperature is above T_{dd}. The measured T_{dd} values for SBS_I, SBS_{II}, and SBS_{III} are 118.9 ± 2.1, 119.9 ± 1.4, and 114.1 ± 1.7 °C, respectively. The tan δ values at the corresponding T_{dd} for all three specimens are similar (note: a vertical shift is applied in Figure 7 for clarity). It seems however that both SBS_I and SBS_{II} have a similar T_{dd}, but SBS_{III} has a relatively small T_{dd}. It has been pointed out that SBS triblock copolymers have a higher order−disorder transition temperature (T_{dd}) than SB diblock copolymers with the same composition and PS sequence length.[14] SBS_{III} specimens with a lower T_{dd} might indicate the presence of a larger amount of mixed phase at the PS/PB interface.[34] This can be confirmed by the T_g shift of the PS phase toward to a lower temperature for SBS_{III}, 82.6 ± 2.7 °C, compared to that for SBS_{II}, 86.8 ± 0.2 °C.

Molecular Characteristics. To reveal the effect of formation conditions on the molecular characteristics of SBS chains, GPC measurements of the as-prepared specimens were carried out to elucidate the molecular weight distribution, as shown in Figure 8. The GPC curves of SBS_I and SBS_{II} are exactly the same as that for the raw SBS materials which show a bimodal molecular weight distribution. One of the distribution peaks is due to the diblock component ($M_w = 7.3 \times 10^4$ g/mol, weight fraction = 0.22); the other is relevant to the triblock component ($M_w = 1.38 \times 10^5$ g/mol, weight fraction = 0.78). Also given in Figure 8 is the GPC result

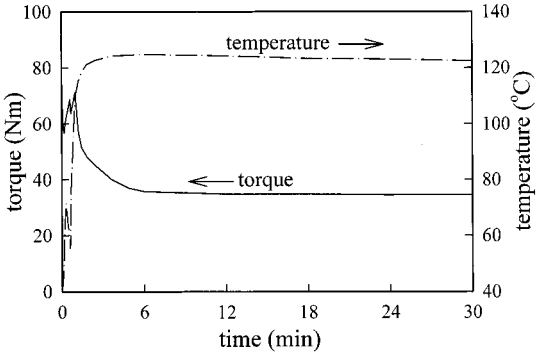

Figure 9. Torque and temperature profiles for SBS melts during melt processing in a Brabender kneader.

for SBS_{III}, suggesting a distinct change of molecular weight distribution after the mixer process. Compared to raw SBS materials, weight fraction of the triblock in SBS_{III} is significantly reduced from 0.78 to 0.47, but the amount of the diblock remains more or less unchanged. In addition, a third distribution peak at higher molecular weight regime ($M_w = 4.2 \times 10^5$ g/mol, weight fraction = 0.14) is observed. Moreover, appearance of species with low molecular weight from 10^4 to 4.0×10^4 ($M_w = 2.8 \times 10^4$ g/mol, weight fraction = 0.12) is evident as well. Since SBS_{III} specimens were melt processed in an internal mixer, prior to being hot-pressed, there must be pronounced effects of molecular friction due to high shear stresses in the mixer on the change of molecular weight distribution.

Figure 9 shows the variation of measured torque in the internal mixer operated at 110 °C and 25 rpm. Also given in Figure 9 is the temperature curve of the SBS melt. A steady-state torque value of 35 N m is detected after mixing for 6 min. Owing to viscous heating by the friction between polymer chains, the measured temperature gradually increases to reach a plateau value of 122 °C, leading to a 12 °C temperature elevation. The significant increase of the melt temperature indicates that large shear stresses are induced in the melt due to the high viscosity. When the stresses are sufficiently high, it is likely to break the backbone chains although SBS molecules are in the terminal region (temperature higher than T_{dd}). The temperature (122 °C) is far from the glass transition of PB phase but slightly above the domain disruption temperature. For triblock SBS chains with flexible PB segments bonded to relatively rigid PS segments at both ends, the most probable location for chain rupture to take place is at the PB chain sequence because of the existence of the unsaturated double bonds in the PB segments. For diblock components, on the other hand, less constraint is imposed on the PB segments due to the free motion at one end so that chain rupture is not observed. Thus, the original diblock content remains more or less unchanged after the mixer process. When one PB segment of triblock chains is broken, however, two free radicals occur and might attack the unsaturated double bonds of neighboring SBS chains to form a larger supermolecule with more than three PS blocks. From the GPC results, large molecules with ca. six PS blocks of equal sequence length are generated after mixing processes to account for the presence of high molecular weight species ($M_w = 4.2 \times 10^5$ g/mol). On the other hand, the low molecular weight species ($M_w = 2.8 \times 10^4$ g/mol) could be produced from the termination of free radicals through disproportionation. Thus, SB diblocks with a short PB segment are developed. The presence of low molecular weight species will raise the miscibility of PS and PB segments which leads to a more mixed phase at the PS/PB interface. It is consistent with the results obtained from RDAII measurements (Figure 7) that show a lower domain disruption temperature for SBS_{III} compared to that for SBS_{II}. Moreover, it is also interesting to note that the loss of entropy resulting from cross-linking of stress-induced radicals to form multiblock copolymers is not sufficiently prominent to change the interdomain distance and the microdomain morphology (Figures 3 and 4).

Correlation between Mechanical Strength and Microstructure. SBS block copolymers are regarded as a composite with rigid cylindrical PS fillers dispersed in the rubbery PB matrix. From a composite point of view, the following parameters have to be considered to determine their performance: properties of the filler and the matrix, the filler/matrix interfacial strength, and the geometrical and spatial characteristics of the fillers, i.e., concentration, size, shape, distribution, and orientation of the fillers. Although different approaches are applied here to prepare SBS specimens, the concentration of PS fillers is the same (volume fraction = 0.24), and the interfacial strength remains unchanged (C−C covalent bonding between PS and PB segments). From the observations of TEM micrographs, a uniform distribution of PS cylinders with equal diameters is found for specimens prepared from different approaches (Figure 4). In addition, no particular orientation of PS cylinders is found globally from either through- or edge-view images. The important parameters left to determine the mechanical strength of SBS specimens are properties of the PS filler and the PB matrix and the shape of PS fillers. Since tear test (or tensile test) is carried out at room temperature at which the PS filler is in the glassy state but the PB matrix is in the rubbery state, the system can be regarded as an elastic PB matrix reinforced with inextensible PS fillers. Thus, the elastic property of PB matrix rather than that of PS fillers plays an important role in determining the composite performance at small strains. Guth[36] proposed a simple relation for composites with an elastic modulus of E as follows:

$$E = E_0(1 + 0.67\phi_s f + 1.62\phi_s^2 f^2) \qquad (5)$$

where E_0 is the elastic modulus of PB matrix, ϕ_s is the volume fraction of PS fillers, and f is the shape factor (a ratio of length to width) of the PS fillers. The magnitude of f stands for the connectivity of the PS microdomains; the larger the f values, the more continuous the PS cylinders dispersed. On the basis of the theoretical rubber elasticity, the elastic modulus of PB matrix, E_0, is closely related to molecular weight between PS microdomains, M_c, and is given by $E_0 = 3\rho_2 RT/M_c$, where ρ_2 is the density of PB matrix, and R and T are the gas constant and the temperature, respectively. Using eq 3 and isooctane solvent to swell the PB phase until the equilibrium swollen state is reached, M_c values for SBS_I, SBS_{II}, and SBS_{III} are determined to be 1.2×10^4, 1.2×10^4, and 9.9×10^3 g/mol, respectively. For SBS_I and SBS_{II} specimens, an identical value of E_0 is expected because the molecular weight between effective cross-linkers (or microdomains) is the same. Since SBS_{II} has a larger elastic modulus

than SBS_I (Table 1), the continuous level of the PS microdomains in SBS_{II} is higher, suggesting a larger f value calculated from eq 5. This is consistent with TEM observations (Figure 4) which show a morphology of more interconnected PS cylinders in SBS_{II}. It is also in agreement with the evaluation of $E'(-125\ °C)/E'(25\ °C)$ ratios obtained from DMA measurements (Table 2), as discussed previously. On the other hand, multiblock copolymers are developed in SBS_{III} to reduce M_c and raise the elastic modulus of the corresponding PB matrix, E_0. Therefore, the elastic modulus of SBS_{III} is larger than that of SBS_{II} (Table 1) although both specimens have similar microdomain morphology.

From Table 1, it is also interesting to note that the breaking stress of SBS_I is the highest although its elastic modulus is the lowest. In contrast to the elastic modulus which is determined from the small strains, breaking stress is highly relevant to the performance at high strains. It has been pointed out that orientation and fragmentation of PS cylinders dominate the mechanical properties at moderate strains.[19−22] If smaller PS fragments are produced, stress concentration in the PB phase will be significantly reduced at high strains, leading to an enhanced stress at break. On this basis, the extraordinarily high breaking stress σ_b for SBS_I may be attributed to the development of finer PS fragments in the bulk after fragmentation, compared to those in SBS_{II} and SBS_{III}. In contrast to SBS_{II}, on the other hand, the reduction of σ_b in SBS_{III} is accounted for the change of triblock content. It should be noted that the mechanical strength of specimens is mainly supported by the triblock components which anchor the PS segments in two different microdomains with PB segments intervening between them. The contribution from diblock components is much limited due to the free dangling of PB segments at one end. Therefore, the reduction of σ_b in SBS_{III} is due to the decrease of the triblock content (Figure 8), after stress-induced degradation, and generation of some amounts of small molecular weight diblock components which is incapable of sustaining the applied load.

On tearing the specimens, orientation and fragmentation of the rigid PS cylinders take place, followed by the rupture of the molecular chains at high strains. The most probable location for chain rupture is at the PS/PB interface due to the stress concentration there and few constraints in the long flexible PB segments. After chain rupture occurs, the failure is likely to proceed along the interface. Because of the presence of the PS fillers (heterogeneity), stick−slip tearing is observed. If the PS cylinders are more interconnected and continuous, larger fragments with irregular shapes are produced so that the crack growing tip will deviate to become more blunt, leading to a higher energy required to proceed the crack growth.[23] On the basis of this consideration, SBS_I should possess the lowest tear strength among the three specimens investigated in this study since the connectivity of PS cylinders is the least. Therefore, on tearing SBS specimens, it is of importance to note that the dominant factor is the failure locus (or microdomain morphology) rather than the intrinsic strength of the block copolymer itself.

Conclusions

Correlation of SBS microstructure to its tear strength would provide valuable insight into the end-use performance of the block copolymer. In this study, tear strengths of SBS block copolymers prepared from three conditions are measured. To reveal any difference resulting from sample preparation, the properties and microstructure of PS and PB phases are systematically determined from various techniques such as TEM, SAXS, DMA, and DSC. Results show that solution-cast specimens possess the lowest tear strength. It is attributed to the microstructure with a relatively ordered pack of PS cylinders, leading to a smooth failure locus when being torn. On the other hand, interconnected PS cylinders are observed in hot-pressed specimens, giving rise to a blunter crack tip on tearing which accounts for a larger tear strength measured. To summary, not only the constituent's properties but also the microdomain morphology play an important role in determining the tear strength of SBS block copolymers.

Acknowledgment. The financial support of this work from National Science Council of Taiwan (NSC86-2216-E-155-003) and from Plastics Industry Development Center (PIDC) is greatly appreciated. Thanks are also due to Professors T.-L. Lin (National Tsing Hua University) and Y. Wang (Tunghai University) for the helps in SAXS and RDAII experiments, respectively. The authors also acknowledge fruitful discussions with Professor S.-M. Lai at CCU. Some of the measurements were carried out by Mr. M.-C. Lin.

References and Notes

(1) Meier, D. J. *J. Polym. Sci., Part C* **1969**, *26*, 81. Also: *J. Polym. Sci., Polym. Phys.* **1996**, *34*, 1821.
(2) Helfand, E.; Wasserman, Z. R. *Macromolecules* **1976**, *9*, 879.
(3) Helfand, E.; Wasserman, Z. R. *Macromolecules* **1978**, *11*, 960.
(4) Helfand, E.; Wasserman, Z. R. *Macromolecules* **1980**, *13*, 994.
(5) Hashimoto, T.; Nagatoshi, K.; Todo, A.; Hasegawa, H.; Kawai, H. *Macromolecules* **1974**, *7*, 365.
(6) Hashimoto, T.; Fujimura, M.; Kawai, H. *Macromolecules* **1980**, *13*, 1660.
(7) Thomas, E. L.; Anderson, D. M.; Henkee, C. S.; Hoffman, D. *Nature* **1988**, *334*, 598.
(8) Hashimoto, T.; Shibayama, M.; Kawai, H. *Macromolecules* **1980**, *13*, 1237.
(9) Séguéla, R.; Prud'homme, J. *Macromolecules* **1978**, *11*, 1007.
(10) Kraus, G.; Rollmann, K. W. *J. Polym. Sci., Polym. Phys.* **1976**, *14*, 1133.
(11) Krause, S.; Lu, Z.-H.; Iskandar, M. *Macromolecules* **1982**, *15*, 1076.
(12) Morèse-Séguéla, B.; St-Jacques, M.; Renaud, J. M.; Prud'homme, J. *Macromolecules* **1980**, *13*, 100.
(13) Denault, J.; Morèse-Séguéla, B.; Séguéla, R.; Prud'homme, J. *Macromolecules* **1990**, *23*, 4658.
(14) Roe, R.-J.; Fishkis, M.; Chang, J. C. *Macromolecules* **1981**, *14*, 1091.
(15) Han, C. D.; Baek, D. M.; Kim, J. K.; Ogawa, T.; Sakamoto, N.; Hashimoto, T. *Macromolecules* **1995**, *28*, 5043.
(16) Sakamoto, N.; Hashimoto, T.; Han, C. D.; Kim, D. Vaidya, N. Y. *Macromolecules* **1997**, *30*, 1621.
(17) Almdal, K.; Koppi, K. A.; Bates, F. S.; Mortensen, K. *Macromolecules* **1992**, *25*, 1743.
(18) Sakurai, S.; Mommi, T.; Taie, K.; Shibayama, M.; Nomura, S. *Macromolecules* **1993**, *26*, 485.
(19) Pakula, T.; Saijo, K.; Kawai, H.; Hashimoto, T. *Macromolecules* **1985**, *18*, 1294.
(20) Séguéla, R.; Prud'homme, J. *Macromolecules* **1988**, *21*, 635.
(21) Sakamoto, J.; Sakurai, S.; Doi, K.; Nomura, S. *Polymer* **1993**, *34*, 4837.
(22) Cohen, Y.; Albalak, R. J.; Dair, B. J.; Capel, M. S.; Thomas, E. L. *Macromolecules* **2000**, *33*, 6502.
(23) Wang, C.; Chang, C.-I. *J. Polym. Sci., Polym. Phys.* **1997**, *35*, 2003.
(24) Wang, C.; Chang, C.-I. *J. Polym. Sci., Polym. Phys.* **1997**, *35*, 2017.
(25) Chen, H.-L.; Hsiao, M.-S. *Macromolecules* **1998**, *31*, 6579.
(26) Flory, P. J.; Rehner, J. *J. Chem. Phys.* **1943**, *18*, 108.
(27) Bishop, E. T.; Davison, S. *J. Polym. Sci., Part* C **1969**, *26*, 59.

(28) Stacer, R. G.; VonMeerwall, E. D.; Kelly, F. N. *Rubber Chem. Technol.* **1985**, *58*, 913.
(29) Gent, A. N.; Lai, S.-M. *J. Polym. Sci., Polym. Phys.* **1994**, *32*, 1543.
(30) Thomas, A. G. *J. Polym. Sci.* **1955**, *18*, 177.
(31) Gent, A. N.; Lai, S.-M.; Nah, C.; Wang, C. *Rubber Chem. Technol.* **1994**, *67*, 610.
(32) Han, C. D.; Baek, D. M.; Kim, J.; Kimishima, K.; Hashimoto, T. *Macromolecules* **1992**, *25*, 3052.
(33) Funaki, Y.; Kumano, K.; Nakao, T.; Jinnai, H.; Yoshida, H.; Kimishima, K.; Tsutsumi, K.; Hirokawa, Y.; Hashimoto, T. *Polymer* **1999**, *40*, 7147.
(34) Nakajima, N. *Rubber Chem. Technol.* **1996**, *69*, 73.
(35) Rosedale, J. H.; Bates, F. S. *Macromolecules* **1990**, *23*, 2329.
(36) Guth, E. *J. Appl. Phys.* **1945**, *16*, 20.

MA011077Q